ELSEVIER

Chemical Engineering Journal 82 (2001) 143–148

Chemical Engineering Journal

www.elsevier.com/locate/cej

Non-isothermal gas–liquid absorption with chemical reaction studies Temperature measurements of a spherical laminar film surface and comparison with a model for the CO_2/NaOH system

M. Taghizadeh, C. Jallut*, M. Tayakout-Fayolle, J. Lieto

Laboratoire d'Automatique et de Génie des Procédés, Université Claude Bernard Lyon 1 et CPE-Lyon, UMR CNRS 5007, 43 Boulevard du 11 Novembre 1918, 69622 Villeurbanne Cedex, France

Received 10 May 2000; accepted 7 October 2000

Abstract

The present work deals with the temperature measurements of a thin spherical liquid film surface during non-isothermal absorption with chemical reaction. The absorption of CO_2 into aqueous NaOH solutions has been used to test the proposed technique. The measurement is based on the use of an infrared pyrometer through a ZnSe window. The experimental results are compared to calculated values obtained from a previously described non-isothermal model. The measured and computed values of the flux of absorbed gas and the temperature profiles are very close without performing any parameter adjustment. The highest measured temperature increase is about 5 K, and despite this low thermal effect, the system has proved to be highly sensitive.

Keywords: Gas–liquid; Chemical reaction; Temperature measurement; Heat transfer; Mass transfer; Modelling

1. Introduction

Gas–liquid absorption with chemical reaction can lead to significant variations of the liquid temperature. In this case, one has to take into account heat transfer for the systems modelling [1]. If all the thermal effects are considered to be concentrated at the gas–liquid interface, rough estimates of the liquid surface temperature rise are available using the film, penetration or surface renewal theories [2–5] and [31]. Temperature variations of rate constant, thermal and mass diffusivities as well as solubility were also taken into account [6–9] and [32]. As far as kinetic studies are concerned, the heat transfer problem was also addressed [10,11] as well as in the case of the design of industrial falling film reactors [12,13] or multiple steady-state analysis [14].

We have been involved into a project for designing fluid curtains to mitigate the consequences of accidental release of toxic gases [15]. Those fluid curtains were considered as open-air reactors and kinetic data had to be gathered for their design. To this end, we have designed and used a spherical absorber and developed an isothermal model for the data reduction [16]. Particularly, we have used our spherical absorber to obtain phosgene absorption data into NaOH aqueous solutions [17]. In this case, we have observed significant rises of the liquid temperature. Therefore, we have modified our apparatus in order to measure the liquid temperature. In the spherical absorber, the liquid, flowing as a thin film from the top to the bottom of the sphere, is brought into contact with a still gas. As the reaction progresses with the angular position or contact time, we have designed a system allowing the measurement of the liquid surface temperature. According to the thickness of the liquid film, the technique has to be non-invasive and is based on the radiation heat transfer properties of the liquid film surface. In the same time, we have developed a non-isothermal model taking into account the heat effects due to the absorption and chemical reactions [11]. We have used the CO_2/NaOH system to test our system.

2. Experimental set-up

The apparatus is represented in Fig. 1. It is adapted from the one described in [16,18]. The absorber is made of an hollow sphere (with a 2×10^{-6} m thick stainless steel wall covered with PTFE) of 6.0×10^{-2} m in diameter, placed into a stainless steel absorption chamber. This chamber is equipped with a ZnSe window transparent to infrared radiations with wavelength between 8×10^{-6} and 12×10^{-6} m [19]. A commercially available calibrated infrared pyro-

* Corresponding author.
E-mail address: jallut@lagep.univ-lyonl.fr (C. Jallut).

1385-8947/01/$ – see front matter
PII: S1385-8947(00)00357-0

Nomenclature

a	liquid thermal diffusivity ($m^2\,s^{-1}$)
c_p	liquid heat capacity ($J\,kg^{-1}\,K^{-1}$)
C	concentration ($mol\,m^{-3}$)
D	mass diffusivity ($m^2\,s^{-1}$)
g	gravity acceleration ($m\,s^{-2}$)
h_g	gas–liquid heat transfer coefficient ($W\,m^{-2}\,K^{-1}$)
H	equilibrium constant ($mol\,m^{-3}\,Pa^{-1}$)
ΔH_r	reaction enthalpy ($J\,mol^{-1}$)
ΔH_s	absorption enthalpy ($J\,mol^{-1}$)
I	ionic strength ($mol\,m^{-3}$)
k	rate constant ($m^3\,mol^{-1}\,s^{-1}$)
P	pressure (Pa)
q_v	liquid volumic flowrate ($m^3\,s^{-1}$)
r_v	chemical reaction rate ($mol\,m^{-3}\,s^{-1}$)
r	radial position in the liquid film (m)
R_0	sphere radius (m)
t_c	gas–liquid contact time (s)
T	temperature (K)
v_r, v_Θ	radial and angular velocities in the liquid film ($m\,s^{-1}$)

Greek letters

λ	liquid thermal conductivity ($W\,m^{-1}\,K^{-1}$)
Δ	liquid film thickness (m)
Θ	angle from the top of the sphere (rad)
ν	liquid kinematic viscosity ($m^2\,s^{-1}$)
ν	stoechiometric coefficient
μ	liquid dynamic viscosity ($kg\,m^{-1}\,s^{-1}$)
ρ	liquid density ($kg\,m^{-3}$)

Subscripts

A	CO_2
B	OH^-
e	electrolyte
g	gas
i	reactant i
ref	reference temperature
w	water
0	liquid inlet

meter has been used to measure the flux emitted through the window. A controlled flowrate of liquid circulates continuously by the mean of a gear pumps (the liquid can also be recycled). It flows around the sphere in the laminar mode. The gas is introduced into the chamber through a sparger filled with water with a flow and a pressure control devices. Table 1 gives the specifications of the main parts of the apparatus.

It is well known that the water transmittivity to infrared radiations is near zero. For example, at 273 K and for 9.3×10^{-6} m, the liquid water emissivity is 0.96 [20]. Consequently, the detector of the pyrometer delivers an electrical signal directly related to the liquid surface temperature. The

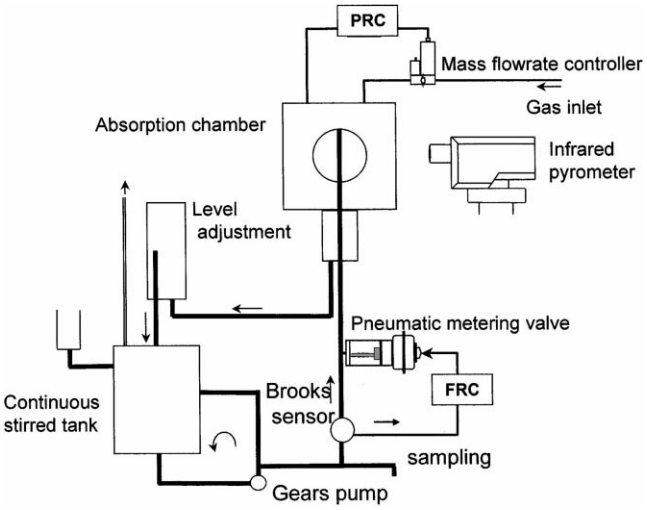

Fig. 1. Experimental apparatus.

use of infrared radiation has already been described within the context non-isothermal gas–liquid studies [21].

The pyrometer support is represented in Fig. 2. The pyrometer can reach five different positions (i.e. five different angles Θ from the top of the sphere) through a vertical displacement whereas an horizontal displacement allows keeping a constant distance between the liquid and the pyrometer. Therefore, the temperature of the liquid surface can be measured with respect to Θ.

3. Experimental results

Absorption experiments of pure CO_2 into aqueous NaOH solutions have been performed according to the following conditions:

- Pure gas pressure: $P_A = 1.018 \times 10^5$ Pa.
- Liquid flow rate: $q_v = 3.333 \times 10^{-6}\,m^3\,s^{-1}$. This value of liquid flow rate leads to a contact time between the gas and the liquid of $t_c = 0.7$ s [17].
- NaOH concentrations: $0.5\,kmol\,m^{-3} < [NaOH] < 2\,kmol\,m^{-3}$.

One can see in the Fig. 3, the evolution of the absorbed gas flux with the liquid inlet NaOH concentration. The flux of absorbed gas increases with the NaOH concentration due to the influence of OH^- ion concentration on the reaction rate (see below).

On the Figs. 4 and 5 are shown the variations of the liquid film surface temperature with Θ and according to the NaOH liquid inlet concentration. The heat effects due to the physical absorption of CO_2 and to the chemical reaction are not very large. The highest temperature rise is obtained for $[NaOH] = 2\,kmol\,m^{-3}$ and is about 5.5 K. Despite this rather low value, our temperature measurement system has proved to be sufficiently sensitive.

Table 1
Main technical characteristics of the experimental set-up

Equipment	Material	Reference	Remarks
Hollow sphere	Stainless steel		Diameter: 0.06 m
Gear pump	Gears in PTFE	MC-Z M886895 Engine: M9935	Maximum flow rate: $4.1 \times 10^{-5}\,m^3\,s^{-1}$ $253\,K < T < 333\,K$
Flow controller for liquid	Stainless steel	Brooks Micro-Oval II LS 4150	Flow rate: 5.5×10^{-7}–$1.1 \times 10^{-5}\,m^3.s^{-1}$ Precision: 1% for $263\,K < T < 353\,K$
Control valve	Stainless steel	Kammer 80037I/P	PID; precision: $\pm 0.25\%$ for $273\,K < T < 323\,K$
Gas flow controller		West 2073	PID; precision: $\pm 0.25\%$ for $273\,K < T < 323\,K$
Pressure sensor	Process side in stainless steel 316	Keller PAA 21	$0 < P < 5 \times 10^{-5}$ Pa; output signal 4–50 mA; precision <20% for $263\,K < T < 353\,K$
Gas mass flow controller		Brooks 5850 TR	$0–3.3 \times 10^{-4}\,m^3\,s^1$ (Nitrogen); precision ±1% of full scale; output signal: 0–5 V
Auto adaptive controller for pressure (master)		West 2073	PID; precision $\pm 0.25\%$ for $273\,K < T < 323\,K$
Gas mass flow controller (slave)		IT 5050	0–5 V
Absorption chamber equipped with a ZnSe window	Stainless steel, ZnSe		$D_{int} = 0.101$ m; $D_{ext} = 0.115$ m; height = 0.190 m; window length = 0.08 m, width = 0.03 m, thickness = 0.004 m
Optical pyrometer		Heimann KT 19	Spectral domain: 8–14 μm; precision: ±0.5 K +0.7% ($T_{amb} - T_{mea}$); temperature domain: 273–373 K; objective: L6; detector: C; output signal 0–20 mA; 24 V ac 50 Hz

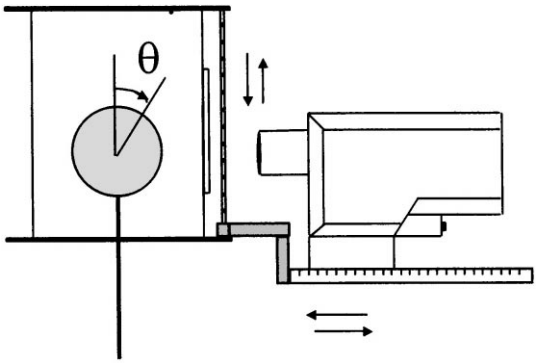

Fig. 2. Details of the absorption chamber and the pyrometer.

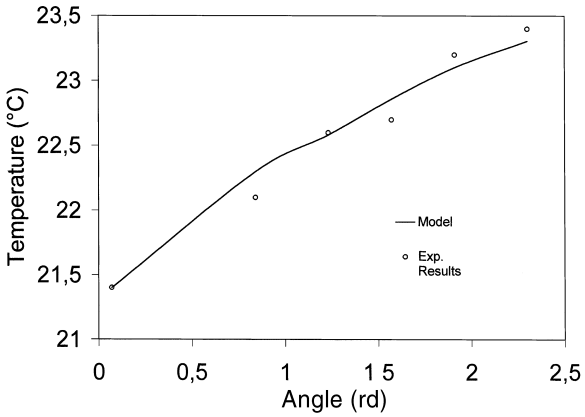

Fig. 4. Measured and calculated variations of the liquid film surface temperature with the angle. Inlet NaOH concentration: 0.5 kmol m^{-3}.

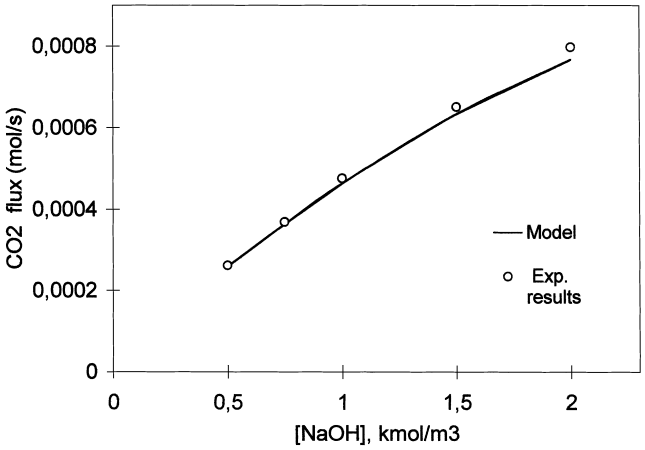

Fig. 3. Measured and calculated variations of the CO_2 absorbed flux with the NaOH inlet concentration.

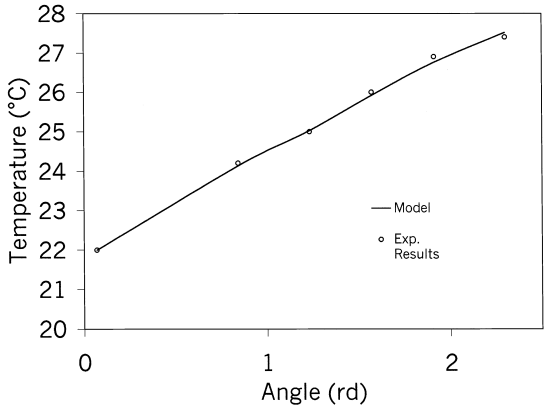

Fig. 5. Measured and calculated variations of the liquid film surface temperature with the angle. Inlet NaOH concentration: 2.0 kmol m^{-3}.

4. Simulation results

4.1. The model

The state variables are assumed to vary only with r, the radial position in the liquid film ($R_0 < r < R_0 + \Delta$) and Θ, the angle from the top of the sphere ($\Theta > \Theta_0$). The thermal and mass diffusivities a and D_i are assumed to be constant. The mass and energy balances are then as follows [11,19].

Component i mass balance

$$v_r \frac{\partial C_i}{\partial r} + \frac{v_\Theta}{r} \frac{\partial C_i}{\partial \Theta} = D_i \left(\frac{\partial^2 C_i}{\partial r^2} + \frac{2}{r} \frac{\partial C_i}{\partial r} \right) + \nu_i r_v \quad (1)$$

Energy balance

$$v_r \frac{\partial T}{\partial r} + \frac{v_\Theta}{r} \frac{\partial T}{\partial \Theta} = a \left(\frac{\partial^2 T}{\partial r^2} + \frac{2}{r} \frac{\partial T}{\partial r} \right) + \frac{r_v(-\Delta H_r)}{\rho c_p} \quad (2)$$

All the liquid phase components i except the absorbed specie A are assumed to be non-volatile. Particularly, one can neglect the solvent evaporation as the gas flows through a sparger before being introduced in the absorption chamber. At steady-state, no heat flux is transmitted toward the hollow part of the sphere which is considered to be a dead-end. The details of the boundary conditions of the problem are given in the Appendix A as well as the velocity profile and liquid film thickness.

The balance equations are solved with the method of orthogonal collocation on finite elements applied to the radial co-ordinate [19,22,23]. Using the DDASPG routine of the IMSL library (Visual Numerics), one solves the resulting algebro–differential equations system.

4.2. CO_2/NaOH system data

This system has been widely studied (see for example [24]) and one can find all the data necessary to perform a simulation study without any parameter adjustment. As far as kinetic data are concerned, we have used the results given in [25]. The limiting step of the reaction is the following:

$$CO_2 + OH^- \rightarrow HCO_3^- \quad (3)$$

which is almost irreversible. This reaction is a second order process and its rate is given by:

$$r_v = k_B C_A C_B \quad (4)$$

At the liquid surface, we assume that CO_2 concentration corresponds to its solubility without chemical reaction. In the reference [25] are given mathematical expressions to calculate the CO_2 solubility as well as the rate constant k_B as functions of the temperature T and the ionic strength I of the solutions. The CO_2 and OH^- diffusivities are assumed to be constant. The CO_2 diffusivity depends on the temperature and electrolytes concentration. A mean value is determined to perform simulations. A constant ratio of 1.7 between the OH^- and CO_2 diffusivities has been adopted [31]. All the details concerning these calculations are given Appendix B. The other properties (fluid viscosity and heat capacity) have been taken from [26,27].

Table 2
Some parameters for the simulation results performed for an NaOH inlet concentration of 1 kmol m^{-3}

Δ_0	0.17×10^{-3} m
Reference temperature, T_{ref}	295 K
CO_2 solubility at $T = T_{ref}$	26.71 mol m^{-3}
CO_2 diffusivity, D_A	1.65×10^{-9} m^2 s^{-1}
OH^- diffusivity, D_B	2.80×10^{-9} m^2 s^{-1}
Heat of reaction, ΔH_r	-89.2 kJ mol^{-1}
Heat of absorption, ΔH_s	-20.3 kJ mol^{-1}
Liquid thermal conductivity, λ	0.597 W m^{-1} K^{-1}
Liquid density, ρ	1043 kg m^{-3}
Liquid viscosity, μ	1.01×10^{-3} Pa s
Liquid thermal capacity, c_p	4005 J kg^{-1} K^{-1}
Gas–liquid heat transfer coefficient, h_g	1 W m^{-2} K^{-1}

The heat of CO_2 dissolution as well the heat of reaction of the overall process

$$CO_2 + 2OH^- \rightarrow CO_3^{2-} + H_2O \quad (5)$$

have been taken from [28].

Table 2 gives the parameters that are used for the calculations reported below. Particularly, one can see that the heat release due to the reaction is 80% of the total one. The liquid thickness at $\theta = \pi/2$ rad is equal to 0.17×10^{-6} m and is almost constant except near the top and the bottom of the sphere. One must notice that the simulation is not valid for $\theta = 0$ rad and $\theta = \pi$ rad (see Appendix A). The gas–liquid heat transfer coefficient h_g has been estimated by assuming that the gas is almost still.

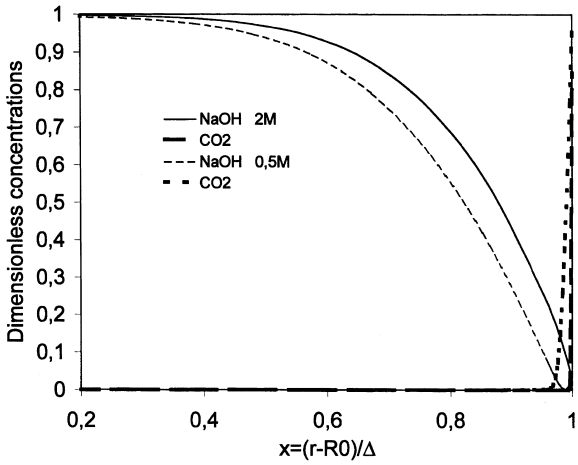

Fig. 6. Examples of simulated reactant profiles for an inlet NaOH concentration of 1 kmol m^{-3}. The concentrations are given under their dimensionless form.

4.3. Comparison with experimental data

One can see on Fig. 6, the CO_2 and NaOH dimensionless profiles calculated at the absorber liquid outlet. CO_2 concentration is normalised by the CO_2 solubility at T_{ref} while the NaOH concentration is normalised by the NaOH inlet concentration. The reaction regime is clearly the instantaneous one at this point.

On Fig. 3 is represented the comparison between the experimental and calculated values of the absorbed CO_2 flux. The calculated and measured liquid surface temperature profiles are given on Figs. 4 and 5 for the two extreme values of the NaOH inlet concentrations that we have explored.

As it can be seen, the model results and the measurements are in good accordance without any adjustment procedure.

5. Conclusion

In this paper, we have presented an experimental technique allowing the measurement of the surface temperature profile of a liquid film involved in a non-isothermal gas–liquid process. A pyrometer sensitive to infrared radiation is used. The measurements are performed through a ZnSe window which is transparent to this radiation.

This technique has been applied to a spherical absorber. Using a moderate exothermal process, the CO_2 absorption into NaOH aqueous solutions, has allowed checking the sensitivity of the measurement technique.

According to the geometry of our system, the comparison of the measurements obtained with the pyrometer with those obtained with another system is very difficult. As a matter of fact, a non-intrusive technique has to be used because of the low thickness of the liquid film. The experimental results are then compared to calculated values obtained from a non-isothermal model of the system. The measured and calculated values of the CO_2 absorption flux and temperature profiles are very close without performing any parameter adjustment. This lead us to conclude that the described technique is well suited to monitor the liquid surface temperature in non-isothermal gas–liquid industrial or pilot plant processes provided that the liquid radiation properties are convenient.

Appendix A

A.1. Boundary conditions

Top of the sphere (film inlet), $\Theta = \Theta_0$ and $R_0 < r < R_0 + \Delta$: $C_A = 0$; $C_i = C_{i0}$; $T = T_0$

Liquid–solid interface, $\Theta > \Theta_0$ and $r = R_0$:

$$\text{Heat transfer } \frac{\partial T}{\partial r} = 0$$

$$\text{Mass transfer } \frac{\partial C_i}{\partial r} = 0$$

Gas–liquid interface, $\Theta > \Theta_0$ and $r = R_0 + \Delta$:

$$\text{Mass transfer } \frac{\partial C_{i\neq A}}{\partial r} = 0$$

$$\text{Solute equilibrium condition } C_A(T) = C_A(T_{ref})\exp\left(\frac{-\Delta H_s}{R}\left(\frac{1}{T} - \frac{1}{T_{ref}}\right)\right)$$

$$\text{Heat transfer } (-\Delta H_s) D_A \frac{\partial C_A}{\partial r} = \lambda \frac{\partial T}{\partial r} + h_g(T - T_g)$$

A.2. Velocity profile and film thickness

They are calculated by using approximate analytical solutions available in the literature [29,30]

$$v_r = -v_r^0 \left(\frac{r - R_0}{\Delta}\right)^2 \left(2 - \frac{r - R_0}{\Delta}\right)$$

$$v_\Theta = v_\Theta^0 \left(1 - \left(1 - \frac{r - R_0}{\Delta}\right)^2\right)$$

with

$$v_\Theta^0 = \left(\frac{3q_V}{4\pi R_0 \Delta_0}\right)(\sin\Theta)^{-1/3}$$

$$v_R^0 = \left(\frac{q_V}{2\pi R_0^2}\right)\cos\Theta(\sin\Theta)^{-2}$$

$$\Delta = \Delta_0 \sin(\Theta)^{-2/3} \text{ with } \Delta_0 \left(\frac{3\nu q_V}{2\pi R_0 g}\right)^{1/3}$$

Appendix B

Rate constant [25]:

$$\log(k_B\ (\mathrm{m^3\,kmol^{-1}\,s^{-1}})) = 11.895 - \frac{2382}{T\ (\mathrm{K})} + 0.221 I\ (\mathrm{kmol\,m^{-3}}) - 0.016(I\ (\mathrm{kmol\,m^{-3}}))^2$$

CO_2 solubility [25]:

$$C_A^* = HP_A$$

with

$$\log\left(\frac{H}{H_w}\right) = -\sum_i I_i h_i$$

$$\log(H_w\ (\mathrm{kmol\,m^{-3}\,kPa^{-1}})) = 9.1229 - 5.9044 \times 10^{-2} T\ (\mathrm{K}) + 7.8857 \times 10^{-5}(T\ (\mathrm{K}))^2$$

and

$$h_{Na^+} = 0.091,\ h_{OH^-} = 0.066,$$
$$h_{CO_3^{2-}} = 0.021, \qquad h_{CO_2} = -0.019$$

Mass diffusivities [25] and [31]

$$D_B = 1.7 D_A$$

$$\frac{D_A}{D_{A_w}} = 1 - 0.129 C_e \ (\text{kmol m}^{-3})$$

$$\log(D_A(\text{m}^2\,\text{s}^{-1})) = -8.1764 + \frac{712.5}{T\ (\text{K})} - \frac{2.591 \times 10^5}{(T\ (\text{K}))^2}$$

References

[1] J. Villadsen, P.H. Nielsen, Models for strongly exothermic absorption and reaction in falling films, Chem. Eng. Sci. 41 (6) (1986) 1655–1671.

[2] G.T. Clegg, R. Mann, A penetration model for gas absorption with first order chemical reaction with first order chemical reaction accompanied by large heat effects, Chem. Eng. Sci. 24 (1969) 321–329.

[3] R. Mann, G.T. Clegg, Gas absorption with an unusual chemical reaction: the chlorination of toluene, Chem. Eng. Sci. 30 (1975) 97–101.

[4] R. Mann, H. Moyes, Exothermic gas absorption with chemical reaction, AIChE J. 23 (1) (1977) 17–23.

[5] C.Y. Chang, D.C. Hwang, Interfacial resistance in exothermic gas absorption with chemical reaction, Chem. Eng. J. 38 (1988) 187–193.

[6] Y.T. Shah, Gas–liquid interface temperature rise in the case of temperature-dependent physical, transport and reaction properties, Chem. Eng. Sci. 27 (1972) 1469–1474.

[7] S. Asai, O.E. Potter, H. Hikita, Nonisothermal gas absorption with chemical reaction, AIChE J. 31 (8) (1985) 1304–1312.

[8] S.G. Chatterjee, E.R. Altwicker, Film and penetration theories for a first-order reaction exothermic gas absorption, Can. J. Chem. Eng. 65 (1987) 454–461.

[9] B.H. Al-Ubaidi, M. Sami Selim, A.A. Shaikh, Nonisothermal gas absorption accompanied by a second-order irreversible reaction, AIChE J. 36 (1) (1990) 141–146.

[10] R. Mann, P. Knysh, J.C. Allan, Exothermic gas absorption with complex reactions: sulfonation and discoloration in the absorption of sulfur trioxide in dodecylbenzene, ACS Symp. Ser. 196 (1982) 441–456.

[11] M. Taghizadeh, C. Jallut, M. Tayakout-Fayolle, J. Lieto, Numerical simulation of non-isothermal gas–liquid absorption with chemical reaction on a spherical laminar film. Application to phosgene absorption into aqueous sodium hydroxyde solutions, Chem. Eng. Sci. 54 (1999) 807–818.

[12] G.R. Johnson, B.L. Crynes, Modelling of a thin-film sulfur trioxyde sulfonation reactor, IEC, Proc. Des. Dev. 13 (1) (1974) 6–14.

[13] E.J. Davis, M. Van Ouverkerk, S. Venkatesh, An analysis of the falling film gas–liquid reactor, Chem. Eng. Sci. 34 (1979) 539–550.

[14] P.H. Nielsen, J. Villadsen, Absorption with exothermic reaction in a falling film column, Chem. Eng. Sci. 38 (9) (1983) 1439–1454.

[15] M. Saint-Georges, J.-M. Buchlin, M.L. Riethmuller, J.P. Lopez, J. Lieto, F. Griolet, Fundamental multidisciplinary study of liquid sprays for absorption of pollutant or toxic clouds, Trans. I. Chem. Eng. 70B (1992) 205–213.

[16] Z. Dehouche, J. Lieto, Modelling and experimental study of key parameters of absorption on wetted sphere contactor, Chem. Eng. Sci. 50 (18) (1995) 2899–2909.

[17] F. Griolet, J. Lieto, G. Astarita, Containment of phosgene accidental release — kinetics of phosgene absorption in sodium hydroxide solution, Chem. Eng. Sci. 51 (12) (1996) 3213–3221.

[18] Z. Dehouche, Conception d'un absorbeur gaz–liquide à film sphérique en vue de la modélisation de cinétiques de transfert de matière avec réactions chimiques, Ph.D. Thesis, Université Claude Bernard, Lyon, France, 1993.

[19] M. Taghizadeh, Etude expérimentale et modélisation de l'absorption réactive non isotherme dans un film laminaire sphérique, Ph.D. Thesis, Université Claude Bernard, Lyon, France, 1998.

[20] J.F. Sacadura, Initiation aux Transferts Thermiques, Lavoisier, Technique et documentation, Paris, 1982.

[21] A.B. Ponter, S. Vijayan, K. Craine, Non-isothermal absorption with chemical reaction-surface temperature and absorption data for the SO_3–H_2SO_4 system, J. Chem. Eng. Jpn. 7 (3) (1974) 225–229.

[22] J. Villadsen, M.L. Michelsen, Solution of Differential Equation Models by Polynomial Approximation, Prentice-Hall, Englewood Cliffs, NJ, 1978.

[23] B.A. Finlayson, Nonlinear Analysis in Chemical Engineering, McGraw-Hill, New York, 1980.

[24] C. Fleisher, S. Becker, G. Eigenberger, Detailed modelling of the chemisorption of CO_2 into NaOH in a bubble column, Chem. Eng. Sci. 51 (10) (1996) 1715–1724.

[25] R. Pohorecki, W. Moniuk, Kinetics of reaction between carbon dioxide and hydroxyl ions in aqueous electrolyte solutions, Chem. Eng. Sci. 43 (7) (1988) 1677–1684.

[26] D.R. Lide, H.P.R. Frederikse, Handbook of Chemistry and Physics, 78th Edition, CRC Press, Boca Raton, FL, 1998.

[27] R.H. Perry, D. Green, Perry's Chemical Engineers' Handbook, MacGraw-Hill, New York, 1984.

[28] D.D. Wagman, W.H. Evans, V.B. Parker, R.H. Schumm, I. Halow, S.M. Bailey, K.L. Churney, R.L. Nuttall, The NBS tables of chemical thermodynamical properties. Selected values for inorganic and C_1 and C_2 organic substances in SI units, J. Phys. Chem. Ref. Data, (2) (1982) 11.

[29] J.F. Davidson, E.J. Cullen, The determination of diffusion coefficients for sparingly soluble gases in liquids, Trans. Inst. Chem. Eng. 35 (1957) 51.

[30] D.C. Gyure, G.T. Clegg, Laminar film flow over a sphere, I.E.C. Fundam. 22 (1983) 405.

[31] P.V. Danckwerts, Gas-liquid reactions, McGraw-Hill, 1970.

[32] A.K. Suresh, S. Asai, O.E. Potter, Temperature-dependent physical properties in physical gas absorption, Chem. Eng. Sci. 38 (1) (1983) 127.